Effective Preprocessing Procedures Virtually Eliminate Distance-Dependent Motion Artifacts in Resting State FMRI

Hang Joon Jo[1],[*], Stephen J. Gotts[2], Richard C. Reynolds[3],
Peter A. Bandettini[1], Alex Martin[2], Robert W. Cox[3], Ziad S. Saad[3]

[1]Section on Functional Imaging Methods, Laboratory of Brain and Cognition, National Institute of Mental Health, National Institutes of Health, Bethesda, MD, USA

[2]Section on Cognitive Neuropsychology, Laboratory of Brain and Cognition, National Institute of Mental Health, National Institutes of Health, Bethesda, MD, USA

[3]Scientific and Statistical Computing Core, National Institute of Mental Health, National Institutes of Health, Bethesda, MD, USA

*Corresponding Author:

Address: 10 Center DR MSC 1148, Building 10 Room 1D80, Bethesda, MD 20892-1148, USA

email: hangjoon.jo@nih.gov

Telephone: +1-301-402-8416

Fax: +1-301-402-1370

Abstract

Artifactual sources of resting-state (RS) FMRI can originate from head motion, physiology, and hardware. Of these sources, motion has received considerable attention and was found to induce corrupting effects by differentially biasing correlations between regions depending on their distance. Numerous corrective approaches have relied on the identification and censoring of high-motion time points and the use of the brain-wide average time series as a nuisance regressor to which the data are orthogonalized (Global Signal Regression, GSReg). We first replicate the previously reported head-motion bias on correlation coefficients using data generously contributed by Power et al. [1]. We then

show that while motion can be the source of artifact in correlations, the distance-dependent bias – taken to be a manifestation of the motion effect on correlation – is exacerbated by the use of GSReg. Put differently, correlation estimates obtained after GSReg are more susceptible to the presence of motion and by extension to the levels of censoring. More generally, the effect of motion on correlation estimates depends on the pre-processing steps leading to the correlation estimate, with certain approaches performing markedly worse than others. For this purpose, we consider various models for RS FMRI preprocessing and show that WMe_{LOCAL}, as subset of the ANATICOR [2] denoising approach results in minimal sensitivity to motion, and reduces by extension the dependence of correlation results on censoring.

Keywords

Functional Magnetic Resonance Imaging, Resting State, Brain Connectivity, Artifact Removal, Head Motion Effect, Preprocessing, Global Signal Regression.

1. Introduction

Resting-State Functional Magnetic Resonance Imaging (RS FMRI) has become a popular methodology for studying brain function with FMRI and holds promise for understanding brain functions without a task or stimulus [3]. A commonly used approach employs the cross correlation between time-series to estimate the strength of connection between a pair of voxels or regions of interest after possible artifacts are removed by linear regression (nuisance-removal regression) from the original echo planar imaging (EPI) time series data. Part of the appeal of RS FMRI is the relative ease with which the data can be acquired.

However, drawing valid inferences can be fraught with pitfalls, as illustrated in recent publications that have caused a considerable stir in the functional neuroimaging field. For example, Power et al. [1] showed that head movement differences between subjects might explain perceived differences in the spatial patterns of brain connectivity and suggested that these motion differences differentially bias short-range versus long-range correlations. This inference was reached by considering the change in inter-regional correlations after high-motion points were eliminated from the estimation of correlation. Removing high-motion samples differentially affected correlations depending on inter-regional distance, thus implicating motion as the source of this distance-dependent bias. As a result, the authors conclude that censoring is the recommended approach for reducing the effects of motion. While we agree with the notion that data censoring can be important, we find that the reported distance-dependent bias is not primarily induced by motion. It is strongly exacerbated by the inclusion of the global signal averaged over whole brain (GS) and related regressors derived by time series averaging over regions containing signals of interest.

In this work, we replicate the bias reported in [1] using the data the authors have very generously made public, we demonstrate how the exclusion of particular tissue-based regressors reduces the distance-dependent bias effect considerably and how the use of a variant on ANATICOR [2] almost entirely eliminates the effect, establishing that our recommended approach is less sensitive to motion induced artifacts. This result is yet another demonstration of why the GS and comparable time series averaged over large brain areas, a practice still widely used, *should not* be projected out of the data in RS-

FMRI [2,4,5]. Finally, we provide an annotated flowchart that presents our recommended data pre-processing pipeline.

2. Materials and Methods

2.1. MRI Data

Image data used in [1] are open to the public at the FCON 1000 project website (http://fcon_1000.projects.nitrc.org). We used children group data (cohort 1; N=22) that exhibited larger motion effects than the other two groups (adolescent and adult cohorts in the full data set). The details of the cohort are described in [1] and the website (http://fcon_1000.projects.nitrc.org/indi/retro/Power2012.html).

2.2. Preprocessing Pipeline

Overview of the preprocessing pipeline for this work is described in Figure 1. The recommended preprocessing steps for RS FMRI analysis are described towards the end of this work (see Figure 7). We deviate from our recommended pipeline to accommodate the particulars of the data at hand, as detailed in the text below and in the flowchart in Figure 1.
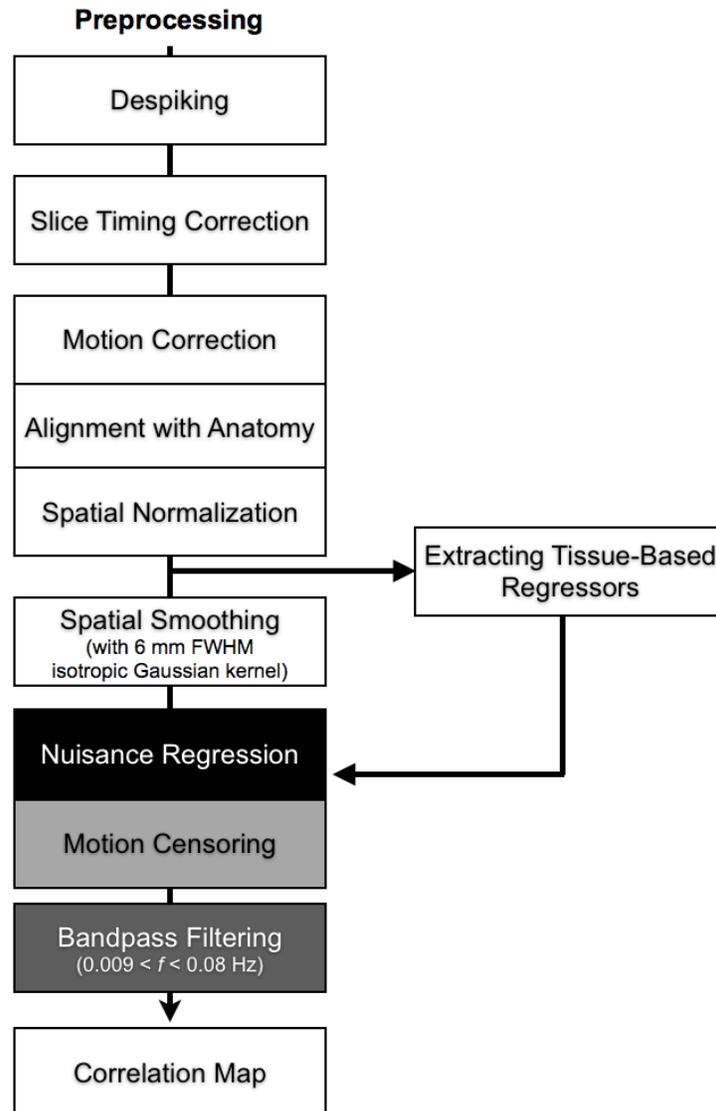
Preprocessing

Figure 1. Overall preprocessing pipeline for this work (see text for detail of each step).

2.2.1. Segmentation of T1-weighted images

T1-weighted images of individual subjects were aligned to the first frame of FMRI echo planar imaging (EPI) data of resting scans, and segmented into gray, white and cerebrospinal fluid tissue classes using AFNI's "*3dSeg*" program [6].

2.2.2. Despiking, Slice-Timing and Head-Motion Correction

Despiking was done with AFNI's "*3dDespike*" program for Figures 2 and 4E, as the first step of the preprocessing pipeline. Each voxel's time series *f(t)* is L^1 fit to a Fourier series of order *L*, defaulting to 1/30 of the number of time points:

$$f(t) = a + bt + ct^2 + \sum_{k=1}^{L} \left\{ d_k \sin\left(2\pi \frac{kt}{T} \right) + e_k \cos\left(2\pi \frac{kt}{T} \right) \right\} \qquad \text{(eq. 1)}$$

where, *T* is the duration of time series, the parameters *a*, *b*, *c*, *d*, and *e* are chosen to minimize the sum over t of $|v(t) - f(t)|$ (L^1 regression), and *v(t)* is the EPI time series of each voxel). The value of *L* used herein is *N*/30, where *N* is the number of time points. The median absolute deviation (MAD) of the residuals is used to obtain a standard deviation estimate σ that is robust to outliers:

$$\sigma = \sqrt{\pi/2}(MAD) \qquad \text{(eq. 2)}$$

For each voxel value, define *s*:

$$s(t) = \frac{v(t) - f(t)}{\sigma} \qquad \text{(eq. 3)}$$

, and values with s greater than the threshold value of *s* for a spike (c_1) are replaced with a value that yields a modified *s'*:

$$s' = c_1 + (c_2 - c_1)\tanh\left(\frac{s - c_1}{c_2 - c_1}\right)$$

<div align="right">(eq. 4)</div>

where, c_2 is the upper range of the allowed deviation from $f(t)$. $s = [c_1, \infty)$ is mapped to s' = $[c_1, c_2)$. By default parameters c_1 and c_2 are set to 2.5 and 4, respectively, although program "*3dDespike*" allows users to modify them. With the default parameters, despiking consists of transforming spike values from the range of $[2.5\sigma, \infty)$ to $[2.5\sigma, 4\sigma)$. The purpose of this transformation is to make the output data be continuous in the input data: small changes in the input (e.g., a value going from slightly under a threshold to slightly over) will not produce large changes in the despiked output. Slice-timing correction was performed, and motion correction was done by rigid body registration of EPI images to a base image [7]. Alignment of EPI data to the T1 was accomplished via an affine transformation, as was the spatial normalization of the T1 to the MNI avg152 T1 template, in MNI stereotaxic coordinates. All 3 transformations were applied at once to the EPI data to prevent multiple resampling steps.

Despiking was skipped in [1]. In practice, however, we find that despiking appears to improve the results of volume registration over time as illustrated in Figure 2 (also see supplementary video S1). With despiking, motion parameters are less variable and the alignment quality is superior when visually examined.
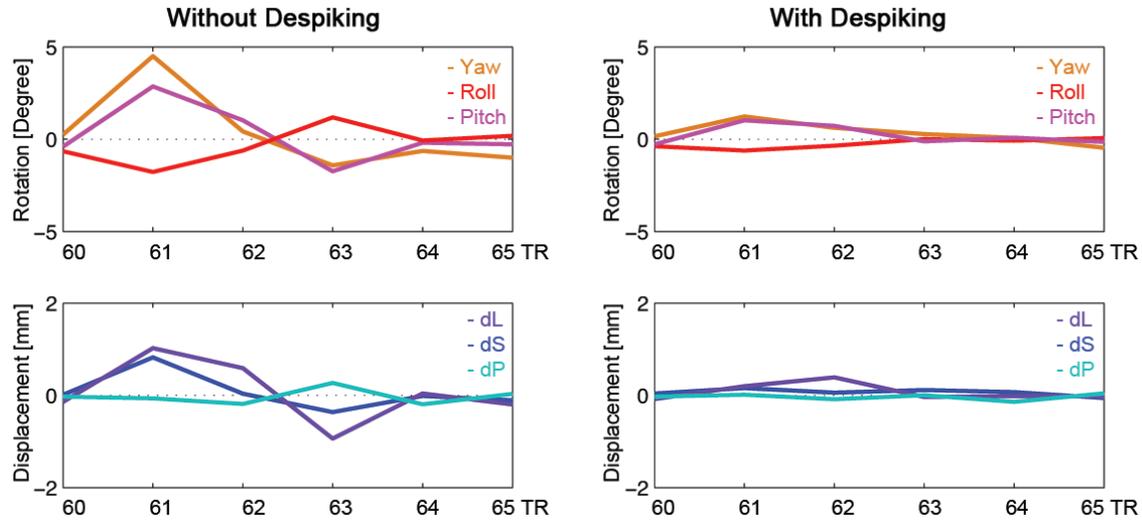
Figure 2. Improved motion correction by adding despiking step. The 6 motion estimates are from time frames in the corresponding video file (Supplementary Material S1). The upper and lower rows show the rotation and translation estimates, respectively, and the left and right columns show the motion estimates from the volume registration of FMRI data processed by pipelines starting without and with despiking, respectively. Registration without despiking resulted in visible residual motion between the 60th to 65th time frames. This suggests that the more elevated motion estimates obtained without despiking are less accurate than those with despiking. The subject used is *sub0015004* of Study 1, who had the largest head movements in the children group.

2.2.3. Nuisance-removal regression

Five types of nuisance regression models were compared in this study. All regressors were extracted from motion-corrected EPI data *before* spatial smoothing with an isotropic Gaussian smoothing kernel (full-width-at-half-maximum; FWHM = 6 mm). Extraction of tissue-based regressors prior to any spatial smoothing is essential, to avoid mixing data from different tissue types; this point, while obvious, is often not made in Methods sections of papers. Regressors in the first model, GS+MO, included: the 6 motion estimates, the tissue-based averages (global signal, GS; white matter signal, WM; large ventricle signal, LV) and the first time difference of each of the aforementioned regressors. In addition, n^{th}-order Legendre polynomials were used to model slow baseline

8

fluctuations. *n* is automatically determined by the number of EPI time points in the AFNI

program *afni_proc.py* and was set to 4 for the time series analyzed here

(http://afni.nimh.nih.gov/pub/dist/doc/program_help/afni_proc.py.html).

$$Y^i = X_{GS}B^i_{GS} + X_{WM}B^i_{WM} + X_{LV}B^i_{LV} + X_{MO}B^i_{MO} + X_{DT}B^i_{DT} + residual \quad \text{(eq. 5; model GS+MO)}$$

where, Y^i is the EPI time series at a voxel i, X_{GS} is a global signal (GS) calculated by

averaging the time-series over all brain mask voxels, X_{WM} is the average signal of all

white matter voxels, X_{LV} are the averaged time series of lateral ventricles (LV) masks,

X_{MO} is the group of six regressors for motion correction parameters (three translation and

three rotation), and X_{DT} is the group of *n* detrending polynomials. The *residual* is the

"cleaned" time series after subtracting the L^2 best-fit regression model of the nuisance

variables from the original voxel time series. The second model, GS, excluded the 6

motion estimate regressors and their first difference terms.

$$Y^i = X_{GS}B^i_{GS} + X_{WM}B^i_{WM} + X_{LV}B^i_{LV} + X_{DT}B^i_{DT} + residual \quad \text{(eq. 6; model GS)}$$

The third model, MO, included motion estimates with their first difference terms but

omitted any tissue-derived regressors and their first difference terms.

$$\text{(eq. 7; model MO)}$$
$$Y^i = X_{MO}B^i_{MO} + X_{DT}B^i_{DT} + residual$$

The fourth model was based on the model MO but included a localized and eroded WM

regressor to form a local estimate of nuisance parameters while avoiding gray matter

signals in the regions of interest.

$$Y^i = X_{MO} B^i_{MO} + X^i_{WMe_{LOCAL}} B^i_{WMe_{LOCAL}} + X_{DT} B^i_{DT} + residual \qquad \text{(eq. 8; model MO+WMe}_{LOCAL}\text{)}$$

where, $X^i_{WMe_{LOCAL}}$ is a regressor of local WM signal for each voxel i, which can be

calculated by averaging signals in eroded WM with a local sphere mask (r=45 mm) by

the AFNI program *3dLocalStat*. The fifth model Depike+MO+WMe$_{LOCAL}$ is based on

the model MO+WMe$_{LOCAL}$, but EPI data Y^i was despiked at the first stage of processing.

These final two models are reduced variants of ANATICOR [2], lacking regressors of

independently acquired physiological signals (not available in [1]) and the eroded large

ventricles (LVe) regressors, as well as the despiking step for the fourth model

(MO+WMe$_{LOCAL}$).

2.2.4. Censoring and bandpass filtering

We based the criterion for censoring on the Euclidian norm of the first time

differences of motion estimates $\|\mathbf{d}\|_2$. This criterion has been part of the AFNI processing

stream (afni_proc.py) and while not identical to the frame-wise displacement (FD) in [1],

it serves the same function of eliminating data at time points when significant rapid

motion is detected. At a $\|\mathbf{d}\|_2$ threshold of 0.25 mm, we censored on average 17.6% of the

time series (1.8% and 45.0% at minimum and maximum, respectively).

Though contrary to our recommendation in the Discussion section, we filtered the

data with a bandpass filtering kernel (0.009 < f < 0.08 Hz) after nuisance regression to

avoid the degrees-of-freedom (DOFs) limitation for high movers because the EPI data had less samples than regression model parameters. This filtering was done via linear regression of sine/cosine basis functions, to avoid artifacts that would otherwise arise from the censoring process (e.g., assuming constant time steps, or including censored data points).

2.2.5. Spatial Smoothing, and Orders of Preprocessing Steps

Figure 3 illustrates the effects of different processing steps on the spectral content of the time series. The preprocessing pipeline used in [1], shown to the left of Figure 3 as pipeline 1, included spatial smoothing (FWHM = 6mm) and bandpass filtering (0.009 - 0.08 Hz) before regression. The first row shows the periodogram of slice-timing and head-motion corrected FMRI data, which were used as the common inputs to both pipelines 1 and 2. The other rows of each column are the periodograms of FMRI data as they are sequentially processed by subcomponents of the pipelines from top to bottom. Gray, black, blue, and red lines are spectral densities of GS, gray matter (GM), cerebrospinal fluid (CSF), and WM masks, respectively, which were averaged across the subjects. Not surprisingly, spatial smoothing can be done at any of these stages, as long as the tissue-based regressors are derived before spatial smoothing. The regression of nuisance parameters can also be carried out either before or after the bandpass filtering stage as long as the nuisance regressors are subject to the same bandpass filter. Otherwise, the regression step would reintroduce frequency components outside of the bandpass range as shown in the bottom row of column 1 [8].
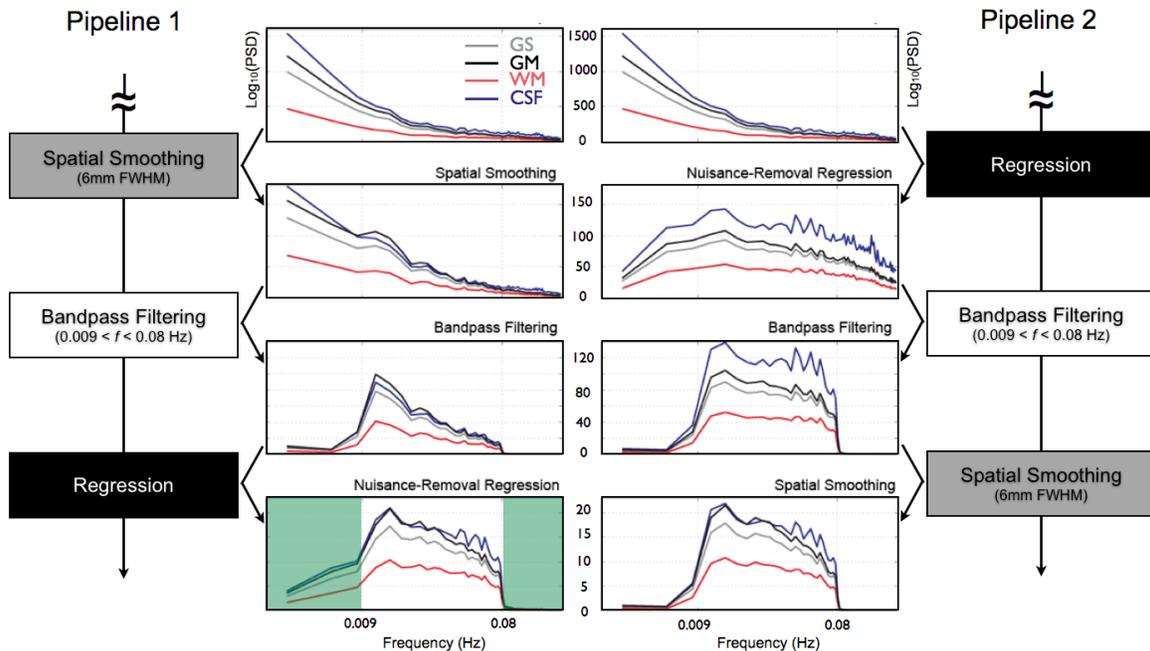
Figure 3. Group averaged power spectrum densities (PSD) of resting-state FMRI time series within brain tissues for each step in two different preprocessing orders. The improper processing order (pipeline 1) can reintroduce noise frequency components (signals of no interest) in lower frequency bands (f<0.009 Hz, the green-tinted area) and higher frequency bands (see the text more details).

2.3. Correlation Analysis for Seed Pairs

For each individual subject, the time series of 264 seed locations in standard brain space (MNI 152) were obtained from censored and uncensored data to produce two sets of 34,716 (264×263/2) Pearson correlation coefficients [1]. The uncensored correlation coefficients were subtracted from the motion-censored correlation coefficients. The correlation differences are plotted as a function of the Euclidean distance between the pairs of seed locations in Figure 4, and the nonlinear dependence on distance is referred to as the distance-dependent correlation bias. Note that for all models, we censored the same fraction of time points. We also examined the benefits of replacing Pearson correlation with Spearman's rank correlation, which is more robust to the presence of outliers in the time series that may be induced by motion.

2.4. Fits of Nuisance Regressors

We examined the spatial distribution of variance captured by the nuisance regressors [4] and correlations between them. To this end, we computed (i) the marginal explained variance (R^2 value) maps of the global signal (GS) and six head-motion estimates (MO) at each voxel in the brain (see Figure 5), and (ii) the cross-correlation matrix of the regressors to identify shared variance (see Figure 6). For these types of tests, the regressors were obtained from the time series that were despiked, slice-timing corrected, and volume registered.

3. Results

3.1. Distance-Dependent Correlation Bias After Different Preprocessing Steps

The distance-dependent correlation biases present after different preprocessing steps are shown in Figure 4, with results for the more standard Pearson correlation coefficient shown in the upper row. The distance dependent bias with the GS+MO model (Figure 4A) mimic those obtained in [1]. The distance-dependent bias is captured by the curvilinear blue trace showing the average change in correlation after censoring. What this result indicates is that the correlation estimate can change considerably in the presence of motion and in a manner that depends on the inter-regional distance. In other words, GS+MO is sensitive to motion and by extension the censoring threshold, since eliminating points of high motion change the correlation values considerably. The desired trend for an estimate in these figures would be a flat line, preferably with zero mean and zero variance as a function of distance. With model GS, where motion estimates with their first difference terms were excluded, the bending of the mean curve was more

pronounced than in Figure 4A (see Figure 4B). With model MO, which included motion estimates and their first differences but excluded tissue-based regressors, the bias was negative throughout and was more constant across inter-regional distances (Figure 4C). Figure 4B and 4C indicate that while the addition of GS makes the correlation estimate more sensitive to motion, the use of MO alone is not enough to yield a robust estimate of correlations. Most notably however, when WMe_{LOCAL} was added as a nuisance regressor to model MO (Figure 4D), the change in correlation became considerably less variable with distance and closer to zero. The addition of despiking further reduced the bias fluctuation as shown in Figure 4E where the nonlinear dependence of bias on distance was mostly eliminated; the mean bias was near zero and the variance of correlation change with censoring was the smallest of all five models tested. Thus of all models tested, $Despike+MO+WMe_{LOCAL}$ resulted in the correlation estimates with minimal sensitivity to the presence of motion.

The lower row of Figure 4 shows results when Spearman's rank was used to compute the correlations. The trends are largely similar to those in Figure 4, with a small reduction in the scatter of correlation change for A, B, C, and D panels where no despiking was performed. Not surprisingly, the use of Spearman's rank had little effect when despiking was included in the processing stages (E).
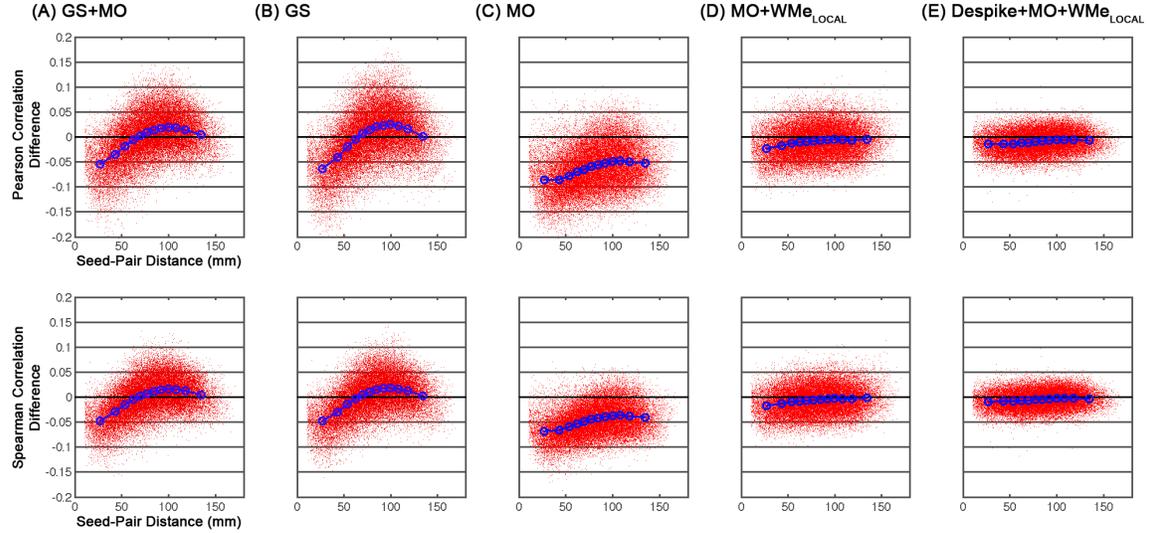
Figure 4. The column (A) shows that censoring high-motion frames from RS-FMRI data decreases short-distance correlations and augments long-distance correlations. The Pearson and Spearman correlation differences are plotted as a function of the Euclidean 3D distance between brain locations in the upper and lower rows, respectively. The results for each seed pair averaged over 22 subjects are plotted as red dots. Blue circles are the grand mean of averaged correlation differences for equal numbers of brain location pairs in twelve segments (2,882 pairs per circle), to highlight the trend. In the preprocessing steps, 6 motion estimates with their first difference terms (MO) and tissue-based regressors with their first difference terms (GS; global, eroded white matter, and lateral ventricle signals) were regressed out. Columns (B) and (C) present the distance-dependent correlation biases of nuisance regression models GS and MO, respectively. Column (D) shows results when a localized and eroded WM signal is added in the regression model of (C). Column (E) shows the model of Column (D) with the addition of despiking. The censored time points of FMRI images were determined at $\|d\|_2 > 0.25$ mm in (A), and the same time points were used in the censoring process of all models.

3.3. GS+MO Regressor Fits

3.3.1. Explained Variances of Nuisance Regressors

The marginal explained variances (R^2 values) of each regressor are presented in Figure 5. For the regression model GS+MO, the regressors (GS and MO) fit most brain regions and locations at the outer edge of the brain with high R^2 values ($R^2>0.3$) (see the column GS+MO in Figure 5). When we measured R^2 values for each regressor, a

15

different pattern in the spatial locations fit by each regressor could be identified: (i) GS tended to fit GM, the sinuses, and mid-sagittal locations (yellow to red color overlays in the column GS in Figure 5; $R^2 > 0.7$), and (ii) MO captured variance more uniformly than GS throughout the brain, and the highest R^2 values were observed along the boundary between cortex and non-brain areas (see the column MO in Figure 5). The areas with the high R^2 values of GS and MO seldom overlapped each other.
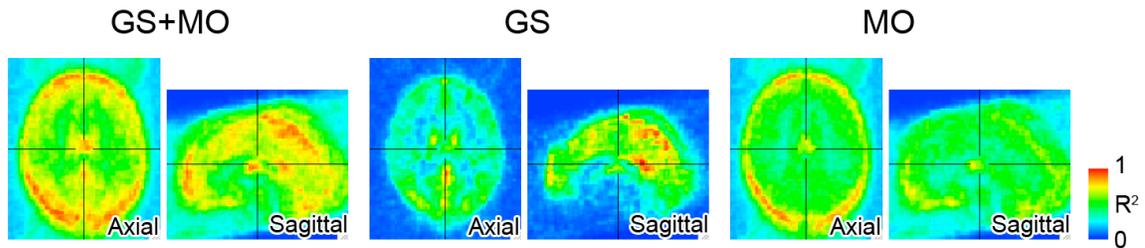

Figure 5. Marginal explained variances (R^2 values) of the regressors in nuisance removal regression models GS+MO. The labels GS and MO correspond to global signal and motion regressors, respectively.

3.3.2. Cross-Correlation Matrix Between Regressors

The cross-correlation matrix between regressors is shown in Figure 6. GS and its first-difference term (GS') only have high correlations with one partial component (*dP*; the displacement along the anterior-to-posterior direction) of MO and its first difference term (MO'), respectively.
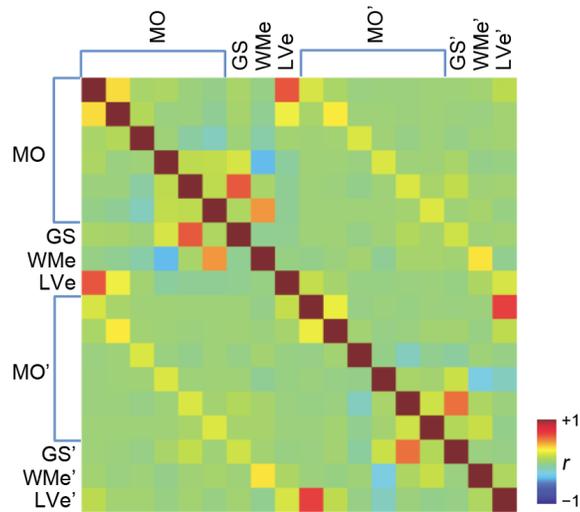
Figure 6. Cross-correlation matrix between the regressors. The correlation coefficients were averaged over all subjects (N=22). MO represents the six regressors containing rigid-body motion parameter estimates (three translations and three rotations). GS is the average RS-FMRI time series over all voxels in the brain mask. WMe and LVe refer to the RS-FMRI time series averaged within eroded white matter and eroded lateral ventricles, respectively. Apostrophe marks (') indicate the first differences of the regressors. The regressors were obtained from the time series that were despiked, slice-timing corrected, and then volume registered, and spatial smoothing *was not* applied to avoid mixing signal across different brain-tissue masks.

4. Discussion

4.1. Correlation Bias Observed by Motion Censoring

It was reported in [1] that the presence of motion introduces a distance-dependent distortion of correlations, whereby correlations between neighboring voxels were biased differently than correlation between voxels that are more distant. The authors also proposed a version (dubbed "scrubbing") of motion censoring as a method to mitigate the bias of motion on correlation estimates. The evidence that the distance-dependent bias was introduced by subject motion was summarized in graphs that show the change in correlation magnitude between a set of brain location pairs (regions-of-interest; ROIs) as

time points affected by excessive motion were excluded from the correlation estimation. The censoring process reduced the distance-dependent bias. While we agree that censoring is a valid approach, we highlight the fact that the distance-dependent bias *does not* appear to be driven by the mere presence of motion, and that the particular choice of preprocessing stream considerably exacerbates this distance-dependent bias. To illustrate this effect, we began by reproducing the effects of data censoring on short- versus long-distance correlations. For Figure 4A, preprocessing included regression of head motion parameters, tissue-based time series including the GS, and their first-order time differences. In a reproduction of the results in [1], we found that censoring differentially affects correlations between ROIs that are close together compared to those that are further apart. This bend in the distribution was considered in [1] as evidence that motion was behind this bias, since lessening the effects of motion through censoring in turn differentially affected correlation values between ROIs depending on their distance. However, this *is not* entirely the case. In Figure 4B, we recomputed the correlation differences but without including the 6 motion estimates and their first differences, thereby amplifying the effect of censoring on the correlations. The scatter plot of the correlation difference increased in variance but the distance-dependent bias remained. The non-linear trends in these scatter plots can be considered as a measure of the sensitivity of particular correlation estimates to motion. The ideal trend for a correlation estimate would be a flattened cloud with small constant variance and a constant bias of 0. In Figure 4C, we brought back the motion estimates with their first differences, but omitted any tissue-derived regressors and their first differences, most notable of which is the GS. With this model, the effect of censoring on the correlations became considerably

less dependent on the inter-ROI distance. The correlation changes were also more

uniformly negative, implying that sharp head motion tends to increase correlations prior

to censoring (see also Gotts et al. [9]). Taking together the results of Figure 4A-C, we

can conclude that the addition of GS to the model exacerbates the distance-dependence of

the correlation estimates on motion, with results that are more dependent on the level of

motion censoring. For Figure 4D, we repeated the analysis in Figure 4C with the

additional inclusion of a local eroded white matter signal, a regressor that intends to

measure local manifestations of artifacts (e.g. hardware artifacts resulting from faulty

head coil channels, [2]) while avoiding regions with the (gray matter) signals of interest.

Not only was the dependence on the inter-ROI distance much reduced, but the mean and

range of the correlation bias were closer to zero. Addition of a despiking step at the very

beginning of the preprocessing pipeline (Figure 4E; see also Satterthwaite et al. [10])

further improved these trends, resulting in correlation estimates that varied little with the

censoring of high-movement data points. The despiking procedure is often used to

dampen the effects of extreme signal deviations on motion correction and variance

estimates, and it is essentially a mild form of censoring. While it is expected that

despiked data will always result in smaller changes in correlation after censoring, the two

operations are not interchangeable as despiking is performed independently for each

voxel. In other terms, not all reduced spikes get flagged as high-motion points. In

conclusion, with a pre-processing model including despiking as an initial processing step

and WMe_{LOCAL}, the correlation estimate was least sensitive to motion artifacts and, by

extension, to censoring threshold levels. We emphasize that the fraction of time points

censored was the same for all the models tested. Even when despiking was adopted in

panel E, we censored the same fraction of time points as in panel A, B, and C. Therefore the fact that censoring had minimal effect on the correlation estimates suggests that the Despike+WMe$_{LOCAL}$ approach is more robust to motion contamination than all the other models and is consequently least sensitive to censoring threshold levels. These results suggest that ANATICOR, the physiological noise augmented form of Despike+WMe$_{LOCAL}$, is not only useful for reducing local hardware artifacts, but also local manifestation of motion. While the basis of the benefit of WMe$_{LOCAL}$ in reducing the motion bias is not entirely clear, one possibility is that it provides some adaptation to small local changes in the B_z magnetic field resulting from movement, which will affect the EPI time series. Lastly, we found that using Spearman rank instead of Pearson correlation was of little advantage for despiked time series but was of mild advantage for other conditions.

4.3. Suggested Preprocessing Pipeline

Figure 7 shows the pipeline we recommend for RS-FMRI analysis. Despiking FMRI data at the subject level is recommended to reduce the contribution of sudden spike signals to correlation estimates. Anecdotally, we also found it to improve the accuracy at the volume registration step (see the video in the supplementary material and Figure 2). Physiological denoising is carried out early in the processing pipeline because RETROICOR [11] nuisance models depend on the acquisition time of each slice relative to the cardiac and respiratory cycles. These nuisance regressors are projected from the timeseries immediately after the despiking step. Bandpass filtering should be applied to both data and regressors of no interest. Otherwise, frequency components in cut-off bands will be introduced back through the regressors of no interest. It is best to perform

censoring, nuisance regression, and bandpass filtering simultaneously in one regression model. By simultaneously doing these three sub-processes in one general linear model, there is no conflict between bandpassing and censoring. Though not carried out in this work for lack of data (physiological measures *were not* taken in [1]), physiological denoising is highly recommended [11,12], as physiological noise differences amongst the subjects can certainly lead to false inferences. In our recommended pipeline in Figure 7, we advocate bandpass filtering in the same model for nuisance regression. This manner of censoring can be handled readily, unlike in the pipelines 1 and 2 of Figure 3.

The regression model used here contains 6 motion estimates, their first difference terms, and WMe_{LOCAL} only, since "global" tissue-based regressors (e.g. GS, average gray matter, GM, non-eroded LV and WM) can also cause group differences either by spreading hardware artifacts that are undetectable by visual inspection in FMRI data [2] or by corrupting the correlation matrix, as can be seen when using GSReg [5]. As long as care is taken to prevent the inclusion of gray matter signals of interest, tissue-based regressors such as eroded LV (LVe) and WMe_{LOCAL} can be beneficial at reducing physiological and hardware artifacts and are part of our recommended ANATICOR [2] approach. The results presented here further demonstrate the utility of WMe_{LOCAL} in helping to reduce head motion artifacts. In these data, we were not able to include timeseries from the LVe mask as a nuisance component because the erosion operation eliminated too many LV voxels in most subjects due to a combination of small brain size and relatively coarse EPI resolution.
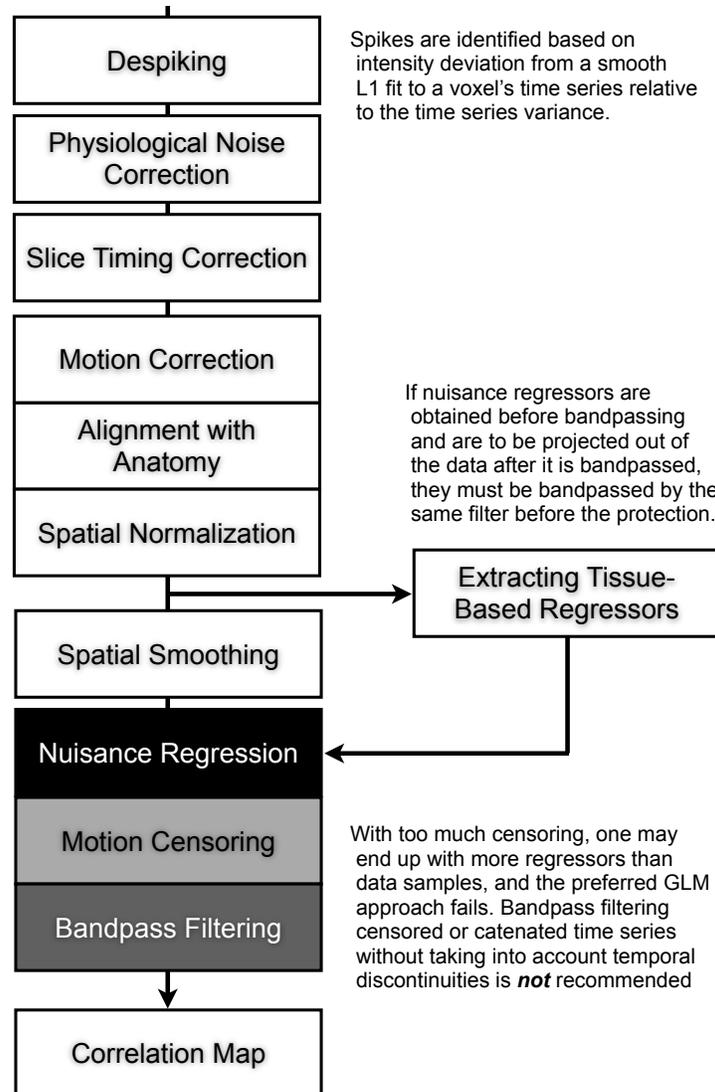
Figure 7. Annotated processing flowchart for RS-FMRI analyses. If nuisance regressors are obtained before bandpassing and are to be projected out of the data after it is bandpassed, they must be bandpassed by the same filter before the projection. With too much censoring, one may end up with more regressors than data samples, and the preferred regression approach fails. Bandpass filtering censored or concatenated time series without taking into account temporal discontinuities *is not* recommended. The WMe$_{LOCAL}$ regressor is recommended, particularly for subject cohorts expected to exhibit high levels of head motion; it has the additional benefit of removing hardware artifacts that are hard to detect visually in the time courses of imaged volumes [2]. Slice-based physiological noise models [11] are projected from the data immediately after the despiking step because they are a function of slice acquisition time. A sample pipeline generating command is shown in example 5C at http://afni.nimh.nih.gov/pub/dist/doc/program_help/afni_proc.py.html).

4.5. Summary

In this work, we have demonstrated that the distance-dependent bias in correlations between ROIs reported by Power and colleagues [1] is not driven only by motion. It is considerably exacerbated by the regression of non-specific, tissue-averaged time series such as the GS. Specifically, the use of GS as a nuisance regressor can increase the sensitivity of correlation estimates to motion and motion censoring levels. This constitutes another example of why GS and equivalent regressors should not be projected out of the data in RS-FMRI [5]. We also find that Despike+WMe$_{LOCAL}$, a reduced version of our denoising approach dubbed ANATICOR [2] resulted in correlation estimates with minimal sensitivity to motion. While many in the field are rightfully concerned about the impact of motion on functional connectivity measures, these concerns can be effectively mitigated by the choice of appropriate preprocessing methods.

Acknowledgments

References

[1] Power, J.D., Barnes, K.A., Snyder, A.Z., Schlaggar, B.L., Petersen, S.E., 2012.

Spurious but systematic correlations in functional connectivity MRI networks arise

from subject motion. Neuroimage 59, 2142-2154.

[2] Jo, H.J., Saad, Z.S., Simmons, W.K., Milbury, L.A., Cox, R.W., 2010. Mapping

sources of correlation in resting state FMRI, with artifact detection and removal.

Neuroimage 52, 571-582.

[3] Biswal, B., Yetkin, F.Z., Haughton, V.M., Hyde, J.S., 1995. Functional connectivity

in the motor cortex of resting human brain using echo-planar MRI. Magn Reson Med

34, 537-541.

[4] Murphy, K., Birn, R.M., Handwerker, D.A., Jones, T.B., Bandettini, P.A., 2009. The

impact of global signal regression on resting state correlations: are anti-correlated

networks introduced? Neuroimage 44, 893-905.

[5] Saad, Z.S., Gotts, S.J., Murphy, K., Chen, G., Jo, H.J., Martin, A., Cox, R.W., 2012.

Trouble at rest: how correlation patterns and group differences become distorted after

global signal regression. Brain Connect 2, 25-32.

[6] Vovk, A., Cox, R.W., Stare, J., Suput, D., Saad, Z.S., 2011. Segmentation priors from

local image properties: without using bias field correction, location-based templates, or

registration. Neuroimage 55, 142-152.

[7] Cox, R.W., Jesmanowicz, A., 1999. Real-time 3D image registration for functional

MRI. Magn Reson Med 42, 1014-1018.

[8] Carp, J., 2011. Optimizing the order of operations for movement scrubbing: Comment on Power et al. Neuroimage. DOI:10.1016/j.neuroimage.2011.12.061

[9] Gotts, S.J., Simmons, W.K., Milbury, L.A., Wallace, G.L., Cox, R.W., Martin, A., 2012, Fractionation of social brain circuits in autism spectrum disorders. Brain 135, 2711-2725.

[10] Satterthwaite, T.D., Elliott, M.A., Gerraty, R.T., Ruparel, K., Loughead, J., Calkins, M.E., Eickhoff, S.B., Hakonarson, H., Gur, R.C., Gur, R.E., Wolf, D.H., 2013. An improved framework for confound regression and filtering for control of motion artifact in the preprocessing of resting-state functional connectivity data. Neuroimage 64, 240-256.

[11] Glover, G.H., Li, T.Q., Ress, D., 2000. Image-based method for retrospective correction of physiological motion effects in fMRI: RETROICOR. Magn Reson Med 44, 162-167.

[12] Birn, R.M., Diamond, J.B., Smith, M.A., Bandettini, P.A., 2006. Separating respiratory-variation-related fluctuations from neuronal-activity-related fluctuations in fMRI. Neuroimage 31, 1536-1548.